Eur. Phys. J. D **31**, 227–237 (2004)
DOI: 10.1140/epjd/e2004-00144-9

THE EUROPEAN PHYSICAL JOURNAL D

Photoassociation experiments with ultracold metastable helium

J. Kim, U.D. Rapol, S. Moal, J. Léonard[a], M. Walhout[b], and M. Leduc[c]

École Normale Supérieure and Collège de France, Laboratoire Kastler Brossel, 24 rue Lhomond, 75231 Paris Cedex 05, France

Received 1st July 2004
Published online 26 October 2004 –

Abstract. The present article gives a review of various photoassociation (PA) experiments performed at ENS with a gas of ultracold atoms of metastable helium in the 2^3S_1 state, using a PA laser beam red-detuned from the 2^3S_1–2^3P transitions. Molecular spectra close to the D_2 atomic line ($2^3S_1 \leftrightarrow 2^3P_2$) are presented. All the measured lines are identified as a signature of molecular bound states having a strong (if not pure) quintet spin character at short interatomic distance. Close to the D_0 atomic line ($2^3S_1 \leftrightarrow 2^3P_0$), giant helium dimers can be produced [see Phys. Rev. Lett. **91**, 073203 (2003)]. A laser set-up improved recently allows us to measure very accurately the binding energy of the ro-vibrational ground state of the 0_u^+ purely long-range potential and the agreement with the theory published previously is excellent. Finally, preliminary results on 2 photon PA spectroscopy are given.

PACS. 32.80.Pj Optical cooling of atoms trapping – 33.20.Kf Visible molecular spectra – 34.50.Gb Electronic excitation and ionization of molecules – 34.20.Cf Interatomic potentials and forces

1 Introduction

Photoassociation (PA) spectroscopy is an appropriate method for acquiring information about the collisional properties of laser-cooled atoms. It provided abundant results for alkali diatomic molecules and allowed the testing of calculations of molecular states and the measurement of lifetimes of excited states with great precision [1]. It also led to precise estimates of the s-wave scattering length [2,3], that rules the interactions between particles in quantum gases and hence most of their collective properties [4].

The present article deals with PA experiments performed with an ultracold gas of ^{4}He atoms in the 2^3S_1 metastable state (denoted He* hereafter). The case of He* is distinctive in that each atom carries a large internal energy of 20 eV, which enables very efficient ionizing collisions, the so-called Penning collisions [5]. However, if the atomic cloud is spin-polarized, this ionization rate is strongly reduced [6–8], higher atomic densities can be achieved and Bose-Einstein Condensation (BEC) is made possible [9,10]. The high internal energy of He* allows for a very efficient detection of the neutral atom He* itself and of the ion rate resulting from Penning collisions inside the cold gas [11]. In addition, with only 2 electrons, ab initio calculations of the atomic fine structure are accurate, which makes He* an appealing candidate for precision spectroscopy and fundamental tests [12]. Finally the absence of hyperfine structure for the ^{4}He isotope is an additional simplification of the molecular photoassociation spectra.

Our group started photoassociation experiments in He* [13] to study the elastic and inelastic collisions in the ultracold gas. Although BEC has been achieved with He*, experimental determinations of the $s-$wave scattering length a are still controversial [9,10,14] with one recent article claiming improved accuracy [15]. Ab initio determinations [16,17] are not accurate enough to provide better accuracy. This uncertainty limits the quantitative study of the collective properties of the ultracold gas like the hydrodynamical modes [18], for instance. Other motivations deal with future experiments where the interactions between atoms could possibly be modified by light [19,20].

Photoassociation experiments with He* were first reported in a Magneto-Optical Trap (MOT) by two groups in The Netherlands [21]. One-photon PA spectra were measured using ion-rate detection. In the present paper, we describe an ensemble of 1- and 2-photon PA experiments performed at ENS under different conditions, that is with a gas of He* atoms magnetically trapped at temperatures close to the BEC transition, and using optical detection. The first section briefly recalls the basis of a molecular analysis used to interpret the PA spectra obtained with a laser operating on the 2^3S_1–2^3P_J lines. The experimental apparatus is described in some detail,

[a] *Present address:* Van der Waals-Zeeman Institute, Universiteit van Amsterdam, The Netherlands.
[b] *Permanent address:* Calvin College, Grand Rapids, MI, USA.
[c] e-mail: leduc@physique.ens.fr

with particular emphasis on the different laser set-ups which are used. The following section gives new results on PA spectra recorded with a laser close to the 2^3S_1–2^3P_2 transition: it provides important complementary information to [21], which gives a new insight into the mechanism of Penning collisions. Section 5 briefly recalls the existence of giant helium dimers in a purely long-range 0_u^+ potential [22]. The binding energy of the ro-vibrational ground state of the 0_u^+ purely long-range potential is measured with improved accuracy. It compares extremely well and confirms earlier theoretical predictions. The last chapter presents prospects on the 2-photon PA experiments in progress, set in order to determine accurately the interaction potential between 2 metastable atoms.

2 Molecular potential curves

Using a PA laser pulse red-detuned with respect to one of the $2^3S_1 \leftrightarrow 2^3P_J$ (D_J) atomic lines ($J = 0, 1, 2$), we can drive a transition from the ${}^5\Sigma_g^+$ electronic state (i.e. a free pair of $2^3S_1 + 2^3S_1$ spin-polarized metastable helium atoms undergoing a collision) to a bound state in an electronic potential connected to one of the 3 asymptotes $2^3S_1 + 2^3P_J$. When the PA laser is resonant with such a free-bound transition, molecules can in principle be produced. This leads secondarily to a drop in the optical density and an increase in the temperature of the cold atomic gas (see Sect. 3.2). Measuring the PA laser frequency for which the optical density of the cloud drops results in a measurement of the energy of the molecular state with respect to the energy of the initial free pair. Since the atomic cloud is so cold (typically 10 μK in our experiment), the energy of the initial free state is well determined and consequently we directly measure the binding energy of the molecule. (Indeed, in our experiment, finite-temperature effects become relevant when the transition energy can be measured to within 1 MHz or less, as discussed in Sect. 5.) The actual production of molecules is then confirmed by the comparison of this experimental molecular spectrum with the calculated one.

The calculation of the binding energies requires the knowledge of the electronic potential curves. In general, the short range part of molecular potentials cannot be calculated exactly. At long interatomic distances however, the molecule can be treated as a two body system, that is two atoms perturbed by their electromagnetic interaction. In the asymptotic case of a $2^3S_1 + 2^3P_J$ helium pair, the perturbation is well approximated by the resonant dipole interaction [23]. The Movre-Pichler approach [24] considers this interaction together with the fine-structure interaction as a perturbation of the non-relativistic atom pair. When applied to the non-rotating $2^3S_1 + 2^3P_J$ helium pair [25], this approach allows for the calculation of the long-range part of the 54 molecular potential curves which are connected to the $2^3S_1 + 2^3P_J$ asymptotes. Partial results are shown Figure 1. Starting from the gerade ${}^5\Sigma_g^+$ states, only ungerade states can be excited in our experiment, and we restrict ourselves to these states in the following.

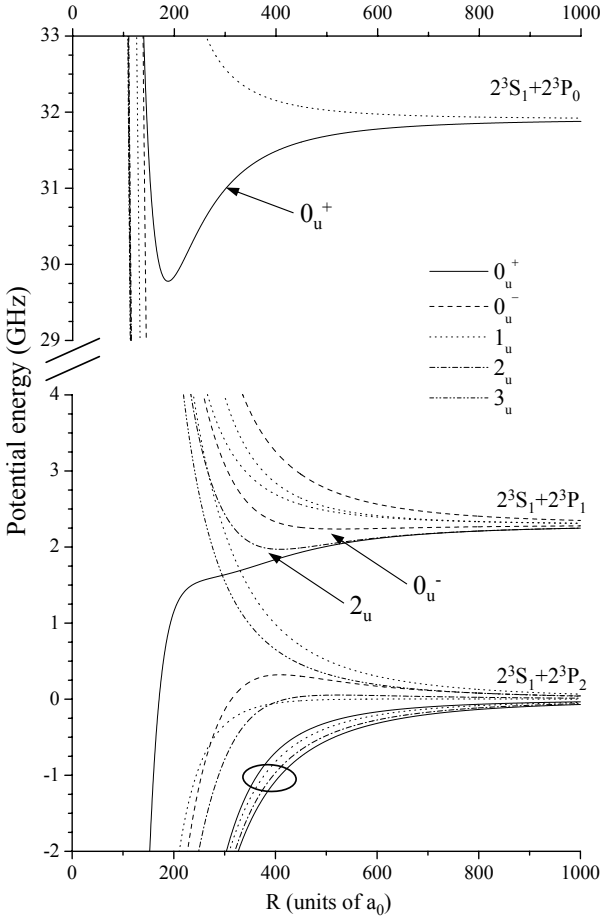

Fig. 1. Ungerade electronic potential curves (in GHz) for the $2^3S + 2^3P_J$ system with fixed nuclei versus the internuclear distance R (in atomic units; 1 $a_0 \simeq 0.0529$ nm), as calculated in [25]. The electronic states are labeled with the projection $\Omega = 0, 1, 2, 3$ of the total electronic angular momentum on the internuclear axis. The quantum numbers $\pm$ and u (ungerade) characterize the properties of the states with respect to the reflection and inversion symmetries, respectively. The ellipse outlines the only four ungerade attractive potential curves connected to the $2^3S_1 + 2^3P_2$ asymptote, that have partly or fully quintet character at short interatomic distance (see Sect. 4). Three arrows indicate the three purely long-range ungerade potential wells (see Sect. 5).

Two different kinds of attractive potential curves appear in Figure 1. First, in most cases the attractive long-range potential curves become repulsive at small interatomic distances, where the Movre-Pichler approach is no longer valid. For the corresponding states, the bound states can not be determined. However, as illustrated in Section 4, the accumulated phase method [26] can be used to take into account the effect of the unknown repulsive part of the potential in the position of the bound states. Then, three attractive long-range potential curves (showed by three arrows in Fig. 1) become repulsive at large distance. The corresponding molecular states are the so-called "purely long-range" states, for which the repulsive part is also due to the resonant dipole interaction.

The existence of a minimum at large distance in these potential curves can be understood as an anti-crossing between one attractive and one repulsive dipole-dipole potential curve due to the atomic fine structure interaction [25]. Giant dimers can be produced in the purely long-range states, and their binding energies can be accurately calculated while taking into account ro-vibrational couplings in between the Movre-Pichler potential curves [25, 27,28]. In Section 5 we show that in the specific case of purely long-range dimers, the agreement between the calculations and the accurate experimental determinations of the binding energies is very good, provided retardation effects are accounted for in the resonant dipole-dipole interaction. In particular we present an improved measurement of the binding energy of the ro-vibrational ground state ($v = 0$) in the $0_u^+, J = 1$ purely long-range potential well.

3 Experimental set-up

3.1 Preparation of the cold cloud

A beam of metastable atoms is generated by a continuous discharge in helium gas cooled at liquid nitrogen temperature. A flux of 2×10^{14} atoms/s/sr, with a velocity of around 1000 m/s, is generated and further decelerated by a Zeeman slower. Atoms are first trapped in a quartz cell by a magneto-optical trap (MOT) [29] using laser beams with a large detuning in view of minimizing the rate of light assisted Penning collisions which destroy the metastable atoms [30]. Then, 5 to 10×10^8 atoms are transferred into a purely magnetic trap of the Ioffe-Pritchard type. A subsequent radio-frequency-induced evaporative cooling sequence cools the gas in 8 s down to the μK range. The metastable atoms can be accumulated at large densities because they are spin-polarized in the trap. Indeed, spin-conservation rules [6] strongly inhibit the Penning ionization when the colliding pairs of atoms are spin polarized (i.e. in a quintet spin state). Bose-Einstein condensation can be reached and the critical temperature is in the range of 1 to 4 μK [9,31], depending on the strength (i.e. oscillation frequencies) of the magnetic trap.

The photoassociation (PA) experiment takes place in the trapped ultracold gas at temperatures slightly above the Bose-Einstein phase transition, in the range 2 to 30 μK. The bias field of the magnetic trap can be varied from 0.1 up to 10 Gauss, which changes the compression and thus the density of the cold gas. For a typical bias field of 4 Gauss and a temperature of 15 μK, the density is of order 10^{13} atoms/cm^3. We illuminate the cloud in the magnetic trap during a few ms with a low-intensity PA beam (see Fig. 2). The PA beam is parallel to the magnetic field and circularly polarized to induce the desired molecular transition.

3.2 Detection

After the PA pulse, a delay of a few 100 ms is introduced before the switching off of the magnetic trap and the detection, so that cloud can thermalize before it is detected.

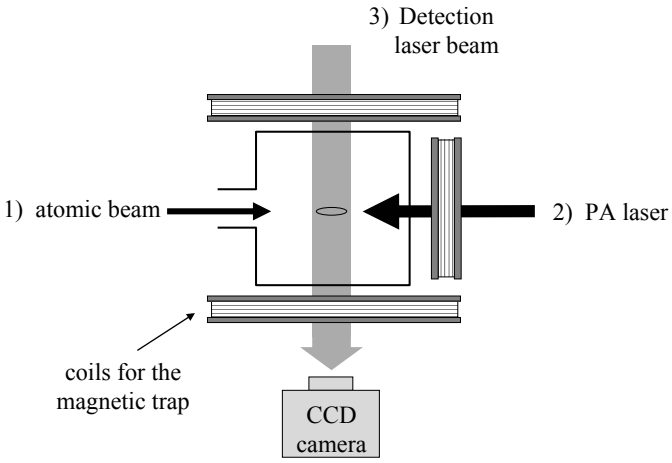

Fig. 2. Experimental set-up. (1) The slow beam of metastable helium atoms loads a MOT. The cloud (represented by an ellipse at the center of the quartz cell) is then cooled by rf-induced evaporation in a 3-coil magnetic trap. (2) The cloud is illuminated inside the trap for a few ms by a PA laser pulse, propagating parallel to the magnetic field. (3) After a few 100 ms the trapping field is switched off and the expanding cloud is imaged on a CCD camera by absorption of a probe beam.

In the present experiment, the detection is optical through the absorption of a resonant probe beam by the cloud. Pictures are recorded with a CCD camera allowing us to measure the trap loss, the optical density and the temperature of the gas deduced from the size of the cloud after a ballistic expansion. When the PA laser is resonant with a molecular transition, we measure a drop in the peak optical density and a strong increase in the temperature of the cloud. The temperature increase allows us to measure precisely the position of the molecular lines.

The heating results from the dissociation of the molecules into pairs of fast atoms, produced with a kinetic energy corresponding to the binding energy of the molecular state. Most of these fast atoms escape from the trap without affecting significantly the cloud but a small fraction of them remains trapped, depending on the trap depth and on the vibrational level that was reached. The trapped fast atoms then thermalize with the cold atomic sample through elastic collisions. The temperature rises with a characteristic thermalization time, depending on the atomic density. This is shown in Figure 3 where the temperature of the gas is plotted as a function of the delay between the PA pulse and the detection pulse. This "calorimetric" detection method thus demands a long enough thermalization time to be effective. In order to understand quantitatively the temperature rise, one has to compare the kinetic energy distribution of the fast atoms to the magnetic trap depth. Orders of magnitude are found satisfactory to explain the observed temperature increase. In addition, it turns out that even a few % photoassociation efficiency leads to a significant temperature rise, whereas the corresponding trap-loss is not detectable. In our experiment, the calorimetric detection method is significantly more sensitive than trap-loss detection.

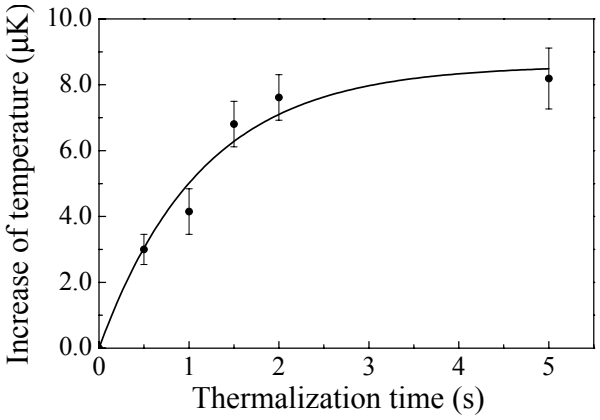

Fig. 3. Heating of the cloud when the PA beam is resonant with a molecular transition. The increase of temperature is plotted as a function of the time delay between the PA illumination and the switching off of the trap and detection pulse. This set of data is obtained with a cloud prepared at 3.5 μK with a density of 3×10^{12} cm^{-3}. The depth of the magnetic trap is 10 mK. The PA pulse has an intensity of $I_{sat}/3$ during 10 ms and is resonant with the transition towards the $v = 2$ level in the 0_u^+ potential (see Sect. 5). An exponential curve with a characteristic time of 1.4 s is fitted to the data.

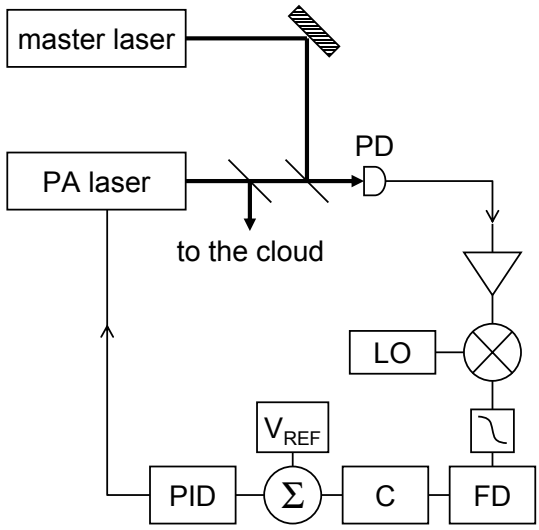

Fig. 4. Laser set-up (III): a reference laser is stabilized on an atomic transition. The beat signal between the master and the PA lasers is detected by a fast photodiode (PD) and amplified, mixed down with a local oscillator (LO), filtered by a low-pass filter, divided by a frequency divider (FD), converted into a voltage by a frequency to voltage convertor (C), compared to a reference voltage (V_{REF}) and finally used by the proportional integrator derivator (PID) for the servo lock of the PA laser.

3.3 Laser set-up

The PA laser beam is produced by a DBR (Distributed Bragg Reflector) diode laser operating on one of the fine structure lines of the $2^3S_1 \leftrightarrow 2^3P$ helium transition. The laser is single mode with a linewidth of 3 MHz without additional frequency narrowing. It can be frequency-tuned without mode hop over more than 600 GHz (i.e. ~ 2.5 nm) by changing the diode temperature. The laser beam is amplified using an ytterbium-doped fiber amplifier, without significant modification of the spectral characteristics. The PA laser beam is triggered and pulsed using Acousto-Optic Modulators (AOM) and sent to the cell via an optical fiber.

A first laser set-up (hereafter called set-up I) is designed for broadband frequency tuning with only a servo-control of the temperature of the diode laser. The laser frequency is measured using a Fabry-Perot cavity, stabilized in temperature. The cavity is injected by both the PA laser beam and a master laser beam stabilized on the D_2 line. The length of the reference cavity is swept over several Free Spectral Ranges (FSR) using a piezo-electric transducer. The comparison between the frequencies of the two lasers is made by counting the number of FSR separating the two frequencies. In this way, the frequency of the PA laser is measured with a typical accuracy of 20 MHz and can be tuned over several 100 GHz. With this laser set-up, we accumulate PA spectra up to 15 GHz to the red of the D_2 line (see Sect. 4).

For an improved frequency stability and precision, we use a second laser set-up (II), for which we put the same diode laser in an external cavity, reducing the linewidth down to 300 kHz. When stabilizing the laser on an atomic transition through saturated absorption spectroscopy, the accuracy of the PA laser frequency is brought to 0.5 MHz. We then tune the PA laser frequency by using 1, 2 or 3 AOM's in series, allowing for an overall detuning ranging between –800 and +800 MHz across an atomic resonance. This set-up is used in the experiments described in [22]. It allows a very accurate measurement of the binding energies of molecular states that are close enough to an atomic transition.

In order to reach larger detunings and keep the precision of the stabilization on an atomic line, we use a third laser set-up (III), similar to that of reference [32]. We again compare the frequency of the PA laser to that of a master laser stabilized on an atomic transition, but we monitor the beat signal between the two lasers (see Fig. 4) with a 2 GHz-bandwidth photodiode and compare it to a local oscillator at 1 GHz. The frequency difference is further divided by a fixed factor and converted into an analog voltage. Finally this voltage is compared with a reference voltage for providing an error signal used to servo lock the current of the PA laser diode. The PA laser frequency can be adjusted by varying the frequency of the local oscillator or the reference voltage. The scanning range is from 0.8 GHz to 1.5 GHz. The accuracy of the PA laser frequency is 0.5 MHz. For a fine scan around the chosen frequency, this set-up can be combined with one or several AOM's. The present device is needed to measure accurately higher binding energies like the one of the $J = 1, v = 0$ ro-vibrational ground state in the 0_u^+ purely long-range potential (see Sect. 5). In the future, we can update this efficient laser set-up with a faster photodiode in order to allow for larger detunings with the same accuracy in the PA laser frequency.

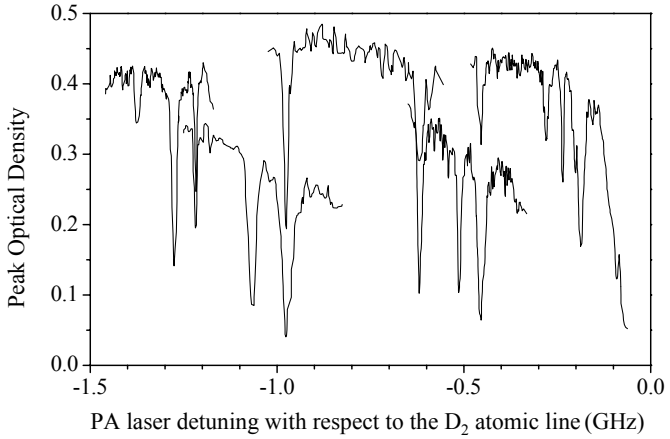

Fig. 5. Example of PA spectra obtained to the red of the D_2 atomic line. The drop in peak optical density results both from trap loss and temperature increase of the sample. The five spectra displayed are obtained with different PA laser exposure times (from 150 ms to 30 ms) and intensities (from $3I_{sat}$ to $I_{sat}/10$). Each spectrum is a series of up to 500 individual data points smoothed by averaging over 5 adjacent points.

4 Molecular spectroscopy to the red of the D_2 transition

We first report on photoassociation experiments performed close to the $2^3S_1-2^3P_2$ helium atomic transition. Similar studies have been carried out in The Netherlands [21] with unpolarized metastable helium atoms accumulated in a MOT at a temperature of order 1 mK and with a detection based on ion rate production monitoring. In our experiment the atomic cloud is 10^3 times denser and the temperature at least 100 times lower. Furthermore the atoms are spin-polarized in the magnetic trap and the detection is optical (see Sect. 3.2). The data are taken using the experimental sequence detailed in Sections 3.1 and 3.2 and the laser set-up (I). Figure 5 displays five sets of experimental data obtained with different intensities and exposure times for the PA laser, in the range from 0 to −1.5 GHz. Importantly, in our experiment a PA spectrum is the result of up to several hundred individual data points, which are each obtained after a full experimental sequence (loading of the MOT, transfer in the magnetic trap, evaporative cooling, PA pulse, thermalization time and detection), which takes typically 20 to 30 seconds. Therefore, in a first attempt, we have accumulated in a systematic way the complete spectrum from the atomic line down to –6 GHz only.

The interpretation of this spectrum is done by assigning each observed PA line to a ro-vibrational level in one of the ungerade electronic potential curves shown in Figure 1. Only molecular states which have quintet spin character at short distance are expected to remain stable against Penning ionization, due to spin conservation rules similar to those mentioned above for colliding metastable atoms. Among the 8 attractive potential accessible to the red of the $2^3S_1 + 2^3P_2$ asymptote, only 4 potentials outlined in an ellipse in Figure 1 are relevant for the interpretation of the molecular spectrum, as they contain a quintet component at short distance. The long-range part of these 4 potentials is 2_u, 1_u and 0_u^+ for two of them. (The other 4 attractive potentials containing only triplet or singlet components lead to an ionization probability equal to unity at very short internuclear distance and can a priori not sustain any bound molecular state.)

Because the short-distance part of the molecular potential is not known accurately, we apply the accumulated phase method [26] to try to assign the PA lines to one or several of the 4 relevant potentials. Close to the dissociation limit, the binding energy of the molecular states is very small compared to the interaction energy at short distance. Consequently, the effect of the inner part of the potential is almost the same for all theses states and the phase of the corresponding radial wavefunctions are almost all identical. For each of the 4 potentials, we integrate inwards the radial Schrödinger equation and we compute the phase of the wave function at fixed internuclear distance $R = 20\ a_0$ (with $a_0 \simeq 0.0529$ nm) for each of the resonance energies detected in the experiment. Our calculation is an elementary one-channel calculation in which only the diagonal part of the rotational couplings are considered, which lead to an independent set of "effective" molecular potentials. No coupling to any ionizing channel is taken into account. Plotting the resulting accumulated phases as a function of the PA laser detuning allows us to identify series of data points which all lead to the same accumulated phase in a given potential. One thus deduces that the corresponding PA lines are the signature of molecular states with increasing vibrational quantum number in this potential.

As an example, Figure 6 shows the calculated accumulated phase at $R = 20\ a_0$, as a function of the binding energies for the 7 lines which are assigned to the $J = 3$ vibrational progression in the 2_u potential. The linear fit has a residual positive slope of 0.012 radian/GHz, which is the first order correction to the assumption of stationarity of the accumulated phase. In fact, from our preliminary spectrum measured up to –6 GHz, only 5 PA lines were found to give a nearly constant accumulated phase in the 2_u, $J = 3$ effective potential curve. The corresponding binding energies are (in GHz): –0.455, –0.98, –1.88, –3.37, –5.64. The existence of this identified series then allowed us to predict the position of other lines in the same potential with larger binding energies: they must also have the same accumulated phase at $R = 20\ a_0$. That is how we could predict and then measure two additional molecular PA lines which are assigned to the same 2_u, $J = 3$ potential with binding energies of –8.95 GHz and –13.67 GHz (see Fig. 6), although we did not make systematic scans at large detunings, as explained above.

Up to now we observed 27 molecular lines to the red of the D_2 atomic transition at the following energies given in GHz with respect to the $2^3S_1 + 2^3P_2$ asymptote: −0.09, −0.185, −0.200, −0.235, −0.280, −0.455, −0.51, −0.62, −0.98, −1.07, −1.22, −1.275, −1.37, −1.88, −2.00, −2.42, −2.59, −3.37, −3.57, −4.25, −4.53, −5.64, −5.90, −7.45, −8.95, −11.70, −13.67. The accuracy of

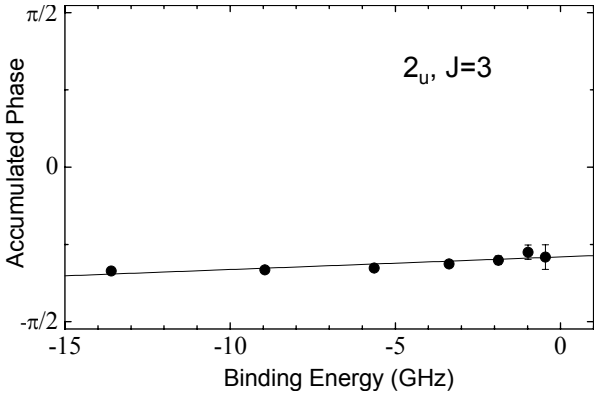

Fig. 6. Plot of the calculated accumulated phase at $R = 20\ a_0$, as a function of the binding energies for the 7 lines corresponding to the $J = 3$ vibrational progression in the 2_u potential. The linear fit has a residual positive slope of 0.012 radian/GHz.

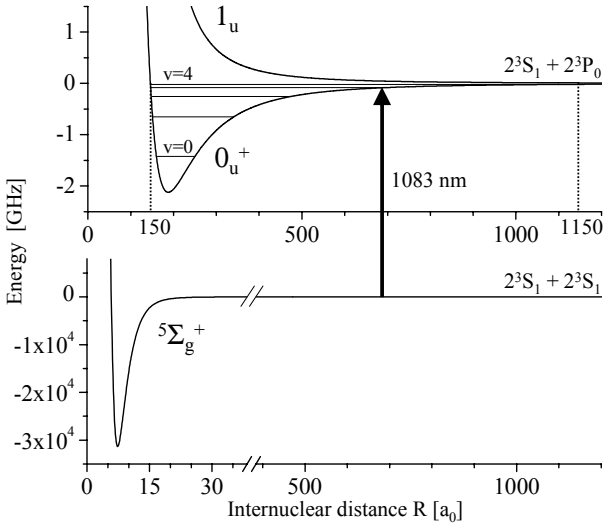

Fig. 7. Molecular potentials involved in the electronic excitation of two 2^3S_1 spin-polarized ^{4}He atoms. The $^5\Sigma_g^+$ potential is taken from [16]. Note the change in energy and length scales between the $^5\Sigma_g^+$ and the purely long-range 0_u^+ potential wells. The excited potentials are taken from [25] and are the only experimentally accessible potentials linked to the $2^3S_1 + 2^3P_0$ asymptote. Five bound states ($v = 0$ to 4) are observed in the 0_u^+ well. Their inner turning points are around 150 a_0, their outer turning points range from 250 a_0 ($v = 0$) to 1150 a_0 ($v = 4$).

these measurements (done with laser set-up I) is 20 MHz. Among those lines, 22 are assigned in the same way to 4 ro-vibrational series in 2 potential curves: 2_u and 1_u. To the level of approximation with which we compute the molecular potentials (see Ref. [25]), these two states become purely quintet at short distances. The 5 unidentified lines have the lowest binding energies (i.e. smallest PA laser detunings), and the experimental accuracy given by laser set-up (I) is not good enough to compute reliable accumulated phases. Our identification technique seems to show that only molecular states which become purely quintet at short distance can produce the PA lines we detect in our experiment.

It is interesting to compare the present results with those of the experiment in Utrecht where ions are detected. After the calibration of the frequency measurement has been corrected in the Utrecht experiment [33], a large number of lines were found at the same PA laser detuning in both experiments. In addition to the ungerade states which are detected in our experiment, the Utrecht group can detect PA lines corresponding to gerade molecular states. On the other hand some molecular states producing fewer ions could not be detected in Utrecht, whereas we detect them. The two experiments at ENS and in Utrecht are largely complementary and a detailed comparison between the results gives new insight into the mechanism of the Penning ionization process. A forthcoming collaboration paper discussing that comparison is being completed [34], leading to more detailed assignments.

5 Accurate spectroscopy in the purely long-range potential to the red of the D_0 transition

Since the purely long-range molecules were first proposed by Stwalley et al. [35], photoassociation spectroscopy of such molecules has been a very powerful tool examining the ground state molecular wave function and for precise determination of s-wave scattering lengths for alkali atoms [36–38]. Purely long-range potentials primarily depend on the leading C_3/R^3 terms of the electric dipole-dipole interaction and on the atomic fine structure which is very accurately determined in the case of ^{4}He in the 2^3P state. Precise calculation of the potential wells and ro-vibrational energies is thus possible [25,28].

Figure 7 shows the long-range part of the potentials that can be excited in our experiment in the vicinity of the D_0 atomic line. The 0_u^+ potential well is purely long-range and contains 6 vibrational levels. The corresponding molecules have inner turning points at internuclear distances larger than 150 a_0 and outer turning points as large as 1150 a_0, which make them the largest diatomic molecules observed so far. Molecules produced by photoassociation of He* are very likely to autoionize due to the same mechanism as the one responsible for Penning ionization. We already mentioned above that Penning collisions are inhibited by spin polarization of the atomic cloud. We now emphasize that purely long-range states is another situation where the autoionization can be avoided. Indeed in a 0_u^+ purely long-range molecule, the two nuclei are never close enough to each other that the autoionization mechanism can occur. This is the reason why the purely long-range dimers were never observed in the Utrecht experiment using exclusively ion-rate detection [39].

In our experiment, calorimetric detection (see Sect. 3.2) allows us to detect purely long-range molecules produced in the 0_u^+ molecular state displayed in Figure 7, when the PA laser is red-detuned from the D_0 atomic line. A typical PA resonance data obtained for the

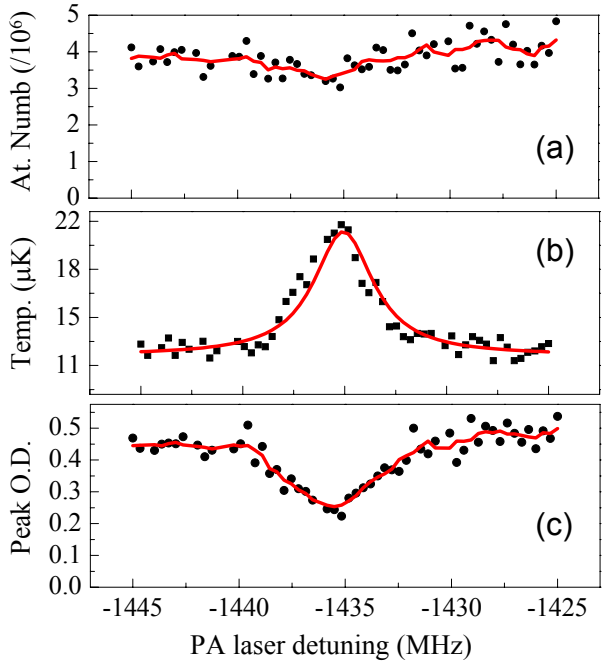

Fig. 8. Detection of the resonant production of the $J = 1$, $v = 0$ ro-vibrational ground state molecules in the 0_u^+ purely long-range potential well. For this experiment the atomic Zeeman energy at the center of the magnetic trap is $\mu B_0 = h\times 8.6$ MHz and the initial temperature of the cloud is $\simeq 12$ μK. After the PA laser pulse (100 ms) and further thermalization (200 ms), the remaining atoms are detected optically (see Sect. 3.2). (a) The number of atoms, (b) the temperature in μK, and (c) the peak optical density of the cold gas are plotted versus the PA laser detuning from the atomic D_0 line. Each point represents a new evaporated cloud after PA pulse illumination, thermalization, and ballistic expansion. The curves in graphs (a) and (c) indicate the averaging of data over five adjacent points. The curve in graph (b) is a Lorentzian fit to the data centered at –1435.0(3) MHz, with a width of 3.6 MHz. Strong heating of the atomic cloud is observed when the PA laser is resonant with a molecular transition.

ro-vibrational ground state ($J = 1, v = 0$) of the 0_u^+ potential well is shown in Figure 8. Although few atoms are lost (Fig. 8a), a strong increase in temperature (Fig. 8b) and consequently a strong decrease in peak optical density (Fig. 8c) are observed. Indeed, since the cloud is very cold (12 μK in the case of Fig. 8), the excitation of relatively few molecules is enough to cause significant heating. Thus, the atomic cloud serves as a sensitive calorimeter capable of detecting the position of the molecular line. This data is obtained with the laser set-up (III) which allows us to tune the PA laser as far as –1.5 GHz and keep an accuracy of 0.5 MHz on the frequency determination.

For an accurate interpretation of the data, we need to take into account the correct line-shape function, which may include shifts and/or asymmetric broadening due to the Zeeman effect (the PA experiments are performed inside the magnetic trap) and the non-zero kinetic energy of the colliding atoms (the trapped gas has finite temperature). Additional shifts due to various mechanisms are negligible in our experimental conditions [25]. To first approximation, the binding energy hb (with h the Planck's constant) of the molecule produced is given by $hb \approx h\delta + 2\mu B_0 + 3k_bT$, where δ is the PA laser detuning corresponding to the center of the PA line, μB_0 is the Zeeman energy of one atom at rest at the center of the trap, and T is the temperature of the gas. Several spectra similar to that of Figure 8 are recorded in different conditions of magnetic field and temperature (see Sect. 3) and finally the binding energy of the ro-vibrational ground state ($J = 1, v = 0$) in the 0_u^+ potential is found to be (in frequency units) $b = -1418.1 \pm 0.5$ MHz.

Table 1. Measured and calculated values of the binding energies in the 0_u^+ potential well for $J = 1$. First column (A) shows the experimental results. The energy of the $v = 0$ state was recently measured with the laser set-up (III) (see Sect. 3.3). The other columns show the results of theoretical calculations with (B) a one-channel calculation obtained by perturbation theory [25], (C) a multi-channel calculation performed with the mapped Fourier grid method [27], and (D) the result of Venturi et al. [28]. All energies are in MHz.

	Experiment	Theory		
v	(A)	(B)	(C)	(D)
5	–	−2.487	−2.59	−2.59
4	-18.2 ± 0.5	−18.12	−18.31	−18.30
3	-79.6 ± 0.5	−79.41	−79.68	−79.65
2	-253.3 ± 0.5	−252.9	−253.17	−253.12
1	-648.5 ± 0.5	−648.3	−648.52	649
0	-1418.1 ± 0.5	−1418	−1417.92	−1418.1
	$(-1430 \pm 20)^a$			

[a] Preliminary value obtained with the laser set-up (I) and reported in [25].

Table 1 recapitulates the binding energies previously measured and calculated in the 0_u^+ potential well for $J = 1$, with the updated experimental result for the $v = 0$ state presented above. The first column (A) shows our experimental results. The other columns show the results of theoretical calculations including retardation effects in the dipole-dipole interaction, with (B) a one-channel calculation obtained by perturbation theory [25], (C) a multi-channel calculation performed with the mapped Fourier grid method [27], and (D) the result of the multi-channel calculation performed by Venturi et al. [28]. For each vibrational level, the measurement and the different theoretical works agree very well. Experimentally the $v = 5$ level is too close to the continuum to be measured, the $v = 4$ to $v = 1$ levels have been measured with laser set-up (II) and already reported in [22], and the $v = 0$ state has been measured at first with laser set-up (I) and more accurately recently with the laser set-up (III).

The new measurement of the $v = 0$ line is the most precise (4×10^{-4} relative uncertainty) of those made for the five bound states detected in the 0_u^+ potential and confirms the excellent agreement between the experimental values and the theoretical predictions. It also provides an essential basis for the future experiment with two-photon

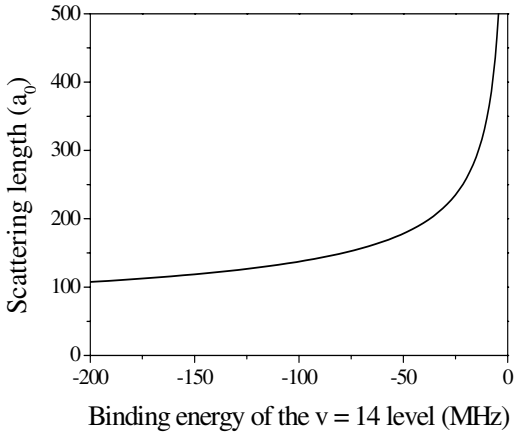

Fig. 9. Scattering length versus the expected binding energy of the least-bound state in the $^5\Sigma_g^+$ potential. The graph is obtained by calculating the binding energy of the least-bound level and the scattering length after varying slightly the attractive part of the potential given in reference [16].

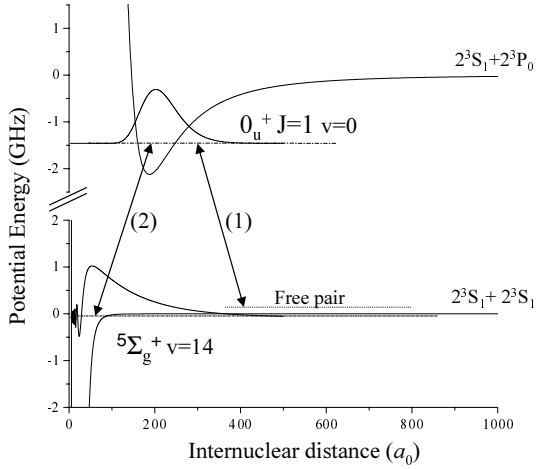

Fig. 10. Schematic of the two-photon photoassociation experiment: a free pair of atoms in the S + S asymptote get excited with laser (1) to an intermediate molecular level of the S + P asymptote (in this case one of the vibrational states in the 0_u^+ potential). The excited molecular state is stimulated to decay into the least bound state of the $^5\Sigma_g^+$ molecular potential by laser (2). The radial wave functions are represented for the final state and the excited intermediate state in the case $v = 0$. The Franck-Condon factor associated to the transition driven by laser (2) is maximal when the 0_u^+ intermediate state is in its ro-vibrational ground state ($J = 1, v = 0$).

photoassociation, in which the ro-vibrational ground state in the 0_u^+ potential is coupled to the weakest bound state in the $^5\Sigma_g^+$ ground state potential (see Sect. 6).

6 Perspective: two-photon PA spectroscopy

Two-photon PA spectroscopy is a powerful probe for the determination of ground-state molecular interaction potentials (see for instance [40]). In particular, accurate determination of the s-wave elastic scattering length a for He* can in principle be obtained with a 2-photon spectroscopic determination of the least-bound vibrational state in the potential, through which two colliding metastable atoms interact. The method has been demonstrated with Lithium atoms by Abraham et al. [2]. In the case of ^{4}He* the binding energy of the least-bound $^5\Sigma_g^+$ state can reasonably be expected between –10 MHz and –150 MHz as shown in Figure 9. This calculation is based on the approximate analytic expression given in reference [16] for the $^5\Sigma_g^+$ potential: the attractive part of this potential is slightly varied within the uncertainty range claimed by the authors, and the corresponding scattering length and least-bound state are calculated. Assuming the scattering length is close to 200 a_0 [15], the graph displayed in Figure 9 suggests that the s-wave scattering length would be determined with a relative accuracy of order 1% provided the binding energy of the least-bound state could be measured within 1 MHz.

Figure 10 illustrates the principle of a possible 2-photon molecular resonance to be observed in order to apply the method above to the case of He*. Photon (1) from a first laser excites a pair of colliding atoms into one of the molecular bound states of the long-range 0_u^+ potential. A second laser (2) drives the transition from this molecular state into the $\nu = 14$ molecular bound state of the $^5\Sigma_g^+$ potential. Our attempts to find a two-photon molecular resonance are directed towards two different paths,

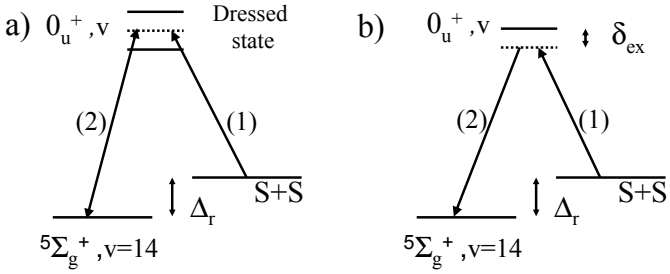

Fig. 11. (a) Frustrated PA scheme: laser (1) resonant with the excited molecular state probes the dressed states created by laser (2). (b) Stimulated Raman scheme: a coherent transfer is driven from the initial pair of free atoms to the least-bound state in $^5\Sigma_g^+$ potential through the intermediate pure long-range state. The frequency of laser (2) is always higher than the one of laser (1).

that are (a) two-photon frustrated photoassociation and (b) two-photon stimulated Raman photoassociation. The level diagram for these schemes is shown in Figure 11.

In the first scheme (Fig. 11a), the frequency of laser (1) is kept fixed on the single-photon PA resonance. According to the detection method explained in Section 3.2, this introduces appreciable drop in the optical density of the atomic cloud. Then, the frequency of laser (2) is scanned and when it becomes resonant with the transition between the two bound states, the upper bound state should undergo the so-called Autler-Townes [20,41] splitting as is described in a dressed-level picture. Consequently, the first photon is brought out of resonance, which should result in a recovery of the optical density signal. This technique has

been successfully applied, for instance to PA experiments in Rb described in [42].

In the second scheme (Fig. 11b), both lasers (1) and (2) are detuned from the molecular level with a common detuning δ_{ex} to the excited molecular state. We denote hereafter Δ_r the frequency difference between the two lasers. If Δ_r matches exactly the energy difference (in frequency units) between the initial (free pair of atom) and the final state (least-bound state in the $^5\Sigma_g^+$ potential), an efficient coherent transfer is expected into the final state [20] if the two lasers are phase locked. These kinds of transitions are expected to have very narrow linewidths dominated by the lifetime of the $^5\Sigma_g^+$ molecules. A rough estimate of the lifetime of these molecules, taking into account only the Penning ionization as the limiting factor, gives a linewidth of the order of 1 MHz. This scheme was employed by Wynar et al. [43] to produce a significant amount of Rb_2 molecules out of a Rb Bose-Einstein Condensate.

In our attempts to find a two-photon molecular resonance we have applied the two techniques above. Preliminary experiments were done with the laser set-up (II), with which the ro-vibrational ground state of the 0_u^+ potential could not be excited. Therefore, the 0_u^+, $J = 1$, $v = 2$ bound state has been chosen to be the excited intermediate state. Based on the $^5\Sigma_g^+$ potential given by [16], modified as explained earlier to reproduce a scattering length close to 200 a_0, the Franck-Condon factor associated with the transition between the excited state and the $v = 14$ molecular state of the $^5\Sigma_g^+$ potential is calculated to be of the order of 10^{-2}. Under these conditions, we are not successful in applying the frustrated photoassociation scheme.

Under the same conditions, the stimulated Raman technique provides some interesting signals. We indeed observe narrow resonances whose widths are as small as 0.5 MHz. However it does not correspond to the molecular resonance we are looking for. In these experiments, the frequency of laser (2) is kept fixed while the frequency of laser (1) is scanned across the PA resonance. A typical optical density signal is shown in Figure 12. The broad decrease in the optical density is due to the production of the $v = 2$ purely long-range state thanks to photon (1). But the narrow dip on the wing of the molecular resonance turns out to be the signature of a Raman resonance between two different spin states of a free pair of metastable atoms, through an intermediate excited state. Photon (1) (propagating parallel to the trapping magnetic field) must be σ^--polarized to excite a pair of trapped atoms in the $0_u{}^+$ purely long-range state. Photon (2) stimulates the intermediate excited state into a free pair of atoms, with a total projection of the final spin state depending on the angular momentum transferred back to the light field. If photon (2) is also σ^--polarized, no dip is visible. If it is π or σ^+ polarized, then the narrow dip appears when the difference Δ_r between the two laser frequencies is equal to once or twice the Zeeman energy μB_0 of one single atom in the field B_0 at the center of the magnetic trap, respectively. This corresponds to a total transfer of 1 or 2 units of angular momentum (respectively) after the 2-photon process has been completed. By varying the value of the fixed frequency of laser (2), we found that the intermediate excited state in this 2-photon process is the atomic state $2^3S_1 + 2^3P_0$, rather than the molecular bound state.

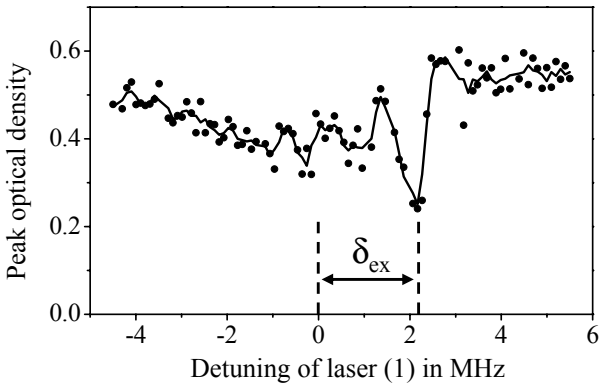

Fig. 12. Observation of a two-photon Raman transition between different spin states of free pairs of colliding metastable atoms. Vertical axis: optical density of the atomic cloud. Horizontal axis: detuning of laser (1) with respect to the one-photon PA resonance corresponding to the $0_u^+, J = 1, v = 2$ molecular state. Two laser beams are applied as shown in Figure 11b. Laser (1) is σ^--polarized and its frequency is scanned. Laser (2) is π-polarized and its frequency is fixed. The solid line is an average over 3 adjacent data points. The sharp dip on the wing of the broad resonance occurs when the difference Δ_r between the two laser frequencies equals the Zeeman energy of one single trapped atom. The distance between the center of the broad resonance and the narrow dip is δ_{ex} as defined in Figure 11b.

The observation of these two-photon transitions between different Zeeman sublevels is encouraging in terms of driving stimulated Raman transitions. Recently we have built laser set-up (III) with which we hope to be able to drive a 2-photon molecular resonance through the ro-vibrational ground state ($J = 1, v = 0$) of the 0_u^+ purely long-range molecule (instead of the $v = 2$ vibrational state used above). The Franck-Condon factor for the transition from this $v = 0$ state to the least-bound state in the $^5\Sigma_g^+$ potential well is estimated to be 10 times larger than from the $v = 2$ state. Also, the $0_u^+, J = 1, v = 0$ state being significantly further detuned from the atomic D_0 line, a larger optical power can be used in photon (2), which should enhance the efficiency of the 2-photon process. The accurate measurement of the binding energy of the $0_u^+, J = 1, v = 0$ state as described in Section 5 is a preliminary result towards new 2-photon experiments which are just starting as we complete the present paper.

7 Conclusion

The present article gives a review of the experimental work which has been carried out on photoassociation in magnetically trapped metastable helium ($^4He^*$) at ENS. PA spectra are recorded using an original "calorimetric" detection method where the temperature of the atomic cold

gas is used as a sensitive probe for the resonant production of molecules. Most of the PA lines observed when the PA laser is red-detuned from the D_2 atomic line have been identified. They correspond to ungerade molecular states which have a purely quintet character at short interatomic distances. All PA lines observed when the PA laser is red-detuned from the D_0 atomic line correspond to the $J = 1$ vibrational progression of the 0_u^+ purely long-range dimer [22]. An accurate measurement of the binding energy of the ro-vibrational ground state ($J = 1, v = 0$) of this dimer has been made possible by the use of laser set-up (III) recently built in our group. It confirms earlier theoretical calculations performed using different approaches.

The work on PA in $^4He^*$ is still in progress. If a 2-photon stimulated Raman signal is obtained between 2 molecular levels, an accurate value of the s-wave scattering length can be expected. The success of this project strongly depends on the lifetime of the least-bound molecular state in the "ground state" potential, which is still unknown. In case this molecular state is observed, the experiment could be reproduced in the Bose-condensed phase. One could thus investigate the possibility to populate a substantial fraction of molecules from the atoms in the condensate.

The results of the present article on the PA spectra close to the D_2 line could be of some practical use in future experiments where we try to modify the interactions between metastable atoms by light, as calculated in [20]. These calculations show that significant changes of the scattering length suppose a very large intensity of the PA beam, and thus a large detuning to avoid prohibitive scattering losses. The existence of relatively long lived molecular states (i.e. somewhat robust against Penning ionization) whose position can be predicted could be exploited in that respect.

Future updates to the present experiment will in any case include important modification of the experimental set-up in order to insert an ion detector in the vacuum system. This would allow for monitoring the ionization rates produced by the Penning collisions in the atomic vapor and by the autoionization of the molecules produced by photoassociation. Such a detection scheme will prove useful as a diagnostic to follow in real time the evolution of the metastable population as well as the production and decay of cold molecules.

The authors would like to thank Claude Cohen-Tannoudji for his constant encouragement and interest in this work. They also thank Allard Mosk, Peter van der Straten and Jeroen Koelemeij for fruitful discussions, Franck Pereira dos Santos and the BNM-SYRTE laboratory for help in building the laser set-up (III). JK acknowledges the post-doctoral fellowship program of Korea Science and Engineering Foundation (KOSEF). UDR acknowledges the postdoctoral grant from the French Ministry of Research. JL acknowledges support from a Marie Curie Intra-European Fellowship (MEIF-CT-2003-501578). MW was partially supported by the National Science Foundation (grant #0140135).

References

1. See e.g. review articles W.C. Stwalley, H. Wang, J. Mol. Spec. **195**, 194 (1999); J. Weiner, V.S. Bagnato, S. Zilio, P.S. Julienne, Rev. Mod. Phys. **71**, 1 (1999); F. Masnou-Seeuws, P. Pillet, Adv. At. Mol. Opt. Phy. **47**, 53 (2001), and references therein
2. E.R.I. Abraham, W.I. McAlexander, C.A. Sackett, R.G. Hulet, Phys. Rev. Lett. **74**, 1315 (1995)
3. J.R. Gardner, R.A. Cline, J.D. Miller, D.J. Heinzen, H.M.J.M. Boesten, B.J. Verhaar, Phys. Rev. Lett. **4**, 3764 (1995)
4. See e.g. L. Pitaevskii, S. Stringari, *Bose-Einstein condensation* (Clarendon Press, Oxford, 2003); C.J. Pethick, H. Smith, *Bose-Einstein condensation in dilute gases* (Cambridge University Press, Cambridge, 2002)
5. A. Niehaus, Adv. Chem. Phys. **45**, 399 (1981)
6. J.C. Hill, L.L. Hatfield, N.D. Stockwell, G.K. Walters, Phys. Rev. A **5**, 189 (1972)
7. N. Herschbach, P.J.J. Tol, W. Hogervorst, W. Vassen, Phys. Rev. A **61**, 050702 (2000)
8. G.V. Shlyapnikov, J.T.M. Walraven, U.M. Rahmanov, M.W. Reynolds, Phys. Rev. Lett. **73**, 3247 (1994)
9. F. Pereira Dos Santos, J. Léonard, Junmin Wang, C.J. Barrelet, F. Perales, E. Rasel, C.S. Unnikrishnan, M. Leduc, C. Cohen-Tannoudji, Phys. Rev. Lett. **86**, 3459 (2001)
10. A. Robert, O. Sirjean, A. Browaeys, J. Poupard, S. Nowak, D. Boiron, C.I. Westbrook, A. Aspect, Science **292**, 463 (2001)
11. S. Seidelin, O. Sirjean, J. Viana Gomes, D. Boiron, C.I. Westbrook, A. Aspect, J. Opt. B **5**, 112 (2003)
12. M.C. George, L.D. Lombardi, E.A. Hessels, Phys. Rev. Lett. **87**, 173002 (2001); J. Castillega, D. Livingston, A. Sanders, D. Shiner, Phys. Rev. Lett. **84**, 4321 (2000); K. Pachucki, J. Sapirstein, J. Phys. B **35**, 1783 (2002)
13. J. Léonard, thèse de Doctorat, Université Marie Curie – Paris 6, 2003, electronic version on line: `http://tel.ccsd.cnrs.fr/`
14. P.J.J. Tol, W. Hogervorst, W. Vassen, Phys. Rev. A **70**, 013404 (2004)
15. S. Seidelin, J.V. Gomes, R. Hoppeler, O. Sirjean, D. Boiron, A. Aspect, C.I. Westbrook, Phys. Rev. Lett. **93**, 090409 (2004)
16. J. Stärck, W. Meyer, Chem. Phys. Lett. **255**, 229 (1994)
17. F.X. Gadéa, T. Leininger, A.S. Dickinson, J. Chem. Phys. **117**, 7122 (2002); A.S. Dickinson, F.X. Gadéa, T. Leininger, J. Phys. B **37**, 587 2004
18. M. Leduc, J. Léonard, F. Pereira Dos Santos, E. Jahier, S. Schwartz, C. Cohen-Tannoudji, Acta Phys. Pol B. **33**, 2213 (2002)
19. P.O. Fedichev, Yu. Kagan, G.V. Shlyapnikov, J.T.M. Walraven, Phys. Rev. Lett. **77**, 2913 (1996); J.L. Bohn, P.S. Julienne, Phys. Rev. A **56**, 1486 (1997)
20. J. Koelemeij, M. Leduc, Eur. Phys. J. D **31**, 263 (2004)
21. N. Herschbach, P.J.J. Tol, W. Vassen, W. Hogervorst, G. Woestenenk, J.W. Thomsen, P. van der Straten, A. Niehaus, Phys. Rev. Lett. **84**, 1874 (2000)
22. J. Léonard, M. Walhout, A.P. Mosk, T. Müller, M. Leduc, C. Cohen-Tannoudji, Phys. Rev. Lett. **91**, 073203 (2003)
23. W.J. Meath, J. Chem. Phys. **48**, 227 (1968)
24. M. Movre, G. Pichler, J. Phys. B **10**, 2631 (1977)

25. J. Léonard, A.P. Mosk, M. Walhout, P. van der Straten, M. Leduc, C. Cohen-Tannoudji, Phys. Rev. A **69**, 032702 (2004)
26. B. Verhaar, K. Gibble, S. Chu, Phys. Rev. A **48**, R3429 (1993); A.J. Moerdijk, W.C. Stwalley, R.G. Hulet, B.J. Verhaar, Phys. Rev. Lett. **72**, 40 (1994)
27. M. Leduc, M. Portier, J. Léonard, M. Walhout, F. Masnou-Seeuws, K. Willner, A. Mosk, *in Proceedings of the XVIth International Conference on Laser Spectroscopy, Palm Cove, Australia, 2003*, edited by P. Hannaford, H.-A. Bachor, K.G. Baldwin, A.I. Sidorov (World Scientific, New Jersey, in press)
28. V. Venturi, P.J. Leo, E. Tiesinga, C.J. Williams, I.B. Whittingham, Phys. Rev. A **68**, 022706 (2003)
29. F. Pereira Dos Santos, F. Perales, J. Léonard, A. Sinatra, J. Wang, F.S. Pavone, E. Rasel, C.S. Unnikrishnan, M. Leduc, Eur. Phys. J. Appl. Phys. **14**, 69 (2001)
30. F. Pereira Dos Santos, F. Perales, J. Léonard, A. Sinatra, J. Wang, F.S. Pavone, E. Rasel, C.S. Unnikrishnan, M. Leduc, Eur. Phys. J. D **14**, 15 (2001)
31. F. Pereira Dos Santos, J. Léonard, Junmin Wang, C.J. Barrelet, F. Perales, E. Rasel, C.S. Unnikrishnan, M. Leduc, C. Cohen-Tannoudji, Eur. Phys. J. D **19**, 103 (2002)
32. T. Stace, A.N. Luiten, R.P. Kovacich, Meas. Sci. Technol. **9**, 1635 (1998)
33. The bindind energies published in [21] are not exact, due to a calibration problem (private communication from P. van der Straten)
34. J. Léonard, P. van der Straten, A.P. Mosk, M. van Rijnbach, M. Walhout, D.Nehari, M. Leduc, in preparation
35. W.C. Stwalley, Y.-H. Uang, G. Pichler, Phys. Rev. Lett. **41**, 1164 (1978)
36. P.D. Lett, P.S. Jullienne, W.D. Phillips, Annu. Rev. Phys. Chem. **46**, 423 (1995)
37. W.C. Stwalley, H. Wang, J. Mol. Spectrosc. **195**, 194 (1999)
38. E. Tiesinga et al., J. Res. Natl. Inst. Stand. Technol. **101**, 505 (1996)
39. P. van der Straten, private communication
40. N. Vanhaecke, Ch. Lisdat, B. TJampens, D. Comparat, A. Crubellier, P. Pillet, Eur. Phys. J. D **28**, 351 (2004)
41. A.H. Autler, C.H. Townes Phys. Rev. **100**, 703 (1955)
42. R.H. Wynar, Ph.D. thesis, University of Texas, Austin USA, 2000
43. R. Wynar, R.S. Freeland, D.J. Han, C. Ryu, D.J. Heinzen, Science **287**, 1016 (2000)